Journal of Materials Chemistry A

PAPER

View Article Online
View Journal | View Issue

Cite this: J. Mater. Chem. A, 2018, 6, 12630

Graphdiyne as an ideal monolayer coating material for lithium-ion battery cathodes with ultralow areal density and ultrafast Li penetration†

Sheng Gong, [b] Shuo Wang, [b] Junyi Liu, [b] Yaguang Guo[ab] and Qian Wang *[ab]

Received 11th March 2018
Accepted 31st May 2018

DOI: 10.1039/c8ta02277a

rsc.li/materials-a

Surface coating of electrodes is an effective way to enhance the performance of lithium-ion batteries (LIBs). It is highly desirable to find ideal coating materials with fast Li penetration and low areal density. Based on first-principles calculations we propose that monolayer sheets can be used as such materials by taking graphdiyne as a test case. We find that the porous structure of graphdiyne can allow fast Li penetration and block the direct contact between the electrode and electrolyte with strong binding between graphdiyne and the $LiCoO_2$ cathode. Graphdiyne has a low areal density, and its electrochemical window is wide enough for it to work at different voltages. In addition, the electronic conductivity of $LiCoO_2$ is improved when coated with graphdiyne as a result of the metallic electronic structure and low interfacial resistance of the graphdiyne coated $LiCoO_2$ electrode. These intriguing theoretical findings would stimulate experimental work on searching for novel coating materials for LIBs.

Introduction

Lithium-ion batteries (LIBs), as the leading energy storage technology, have been intensively studied for decades.[1] However, several issues still exist that affect the performance of LIBs, including the undesirable reactions from direct contact between electrodes and electrolytes,[2] strain induced cracking and pulverization of electrodes[3] and poor electron kinetics of semiconducting electrodes.[4] To improve the electrochemical performance of electrodes, surface coating has been widely used to block the direct contact between electrodes and electrolytes,[2,5,6] and in some cases it can also improve the mechanical and structural stability,[3,5] and the surface electronic conductivity of electrodes.[7] It has been demonstrated that an ideal coating material needs to meet some basic requirements: (1) tight bonding with electrodes,[5] (2) light mass and high chemical and electrochemical stability, and low areal density[5,8] and (3) fast Li conduction and slow electrolyte penetration,[2,9] while it is also expected to achieve multifunctionalities.[10] In this sense, most metal oxides should not be seen as ideal coatings due to their poor electronic and ionic conductivity,[2,11] while traditional carbon coatings are thick and heavy, which would reduce specific capacity and result in slower Li kinetics.[3,5,6] Here, we propose that thin and light monolayers could have the potential to be used as coatings, and find that graphdiyne[12] would be one of the best coating materials. Unlike pristine graphene, which has a high penetration barrier of 9.71 eV,[13] graphdiyne is penetrable by Li without a penetration barrier when used as an anode,[14] and has an ultralow areal density of 0.47 mg m^{-2} that is only 68% of that for graphene.[15] Moreover, graphdiyne is found to be both mechanically strong and ductile,[16] which can improve the strength of coated particles.[15] It also has high chemical stability,[17] and can remain stable under an O_2-rich environment.[18] In addition, the realization of particles encapsulated by monolayers, such as non-precious metals coated with graphene[19] and Co oxides coated with a g-CN monolayer,[20] suggests that it is technologically feasible to coat electrodes with graphdiyne.

In this work, we conduct first-principles calculations to investigate the transport behaviors of Li and the ethylene carbonate molecule, the smallest molecule among the widely used organic electrolytes,[1] through the pores in graphdiyne. We also calculate the electrochemical window of graphdiyne to evaluate its electrochemical stability, and then coat graphdiyne on the $LiCoO_2$ cathode to study the bonding and electronic properties of the stacked heterostructure. Our results show that the graphdiyne coating layer allows ultrafast Li penetration and effectively blocks the contact between the electrolyte and the electrode with a wide electrochemical window, proving the high electrochemical stability of graphdiyne, and the electronic conductivity of the $LiCoO_2$ cathode is improved with tight bonding between graphdiyne and the $LiCoO_2$ surface.

Computational methods

All the quantum mechanical calculations are conducted based on density functional theory (DFT), as implemented in the

[a]Center for Applied Physics and Technology, BKL-MEMD, College of Engineering, Peking University, Beijing 100871, China. E-mail: qianwang2@pku.edu.cn

[b]Department of Materials Science and Engineering, College of Engineering, Peking University, Beijing 100871, China

† Electronic supplementary information (ESI) available. See DOI: 10.1039/c8ta02277a

Vienna *ab initio* Simulation Package (VASP).[21] The projector augmented wave (PAW) method[22] is employed with a kinetic energy cutoff of 500 eV,[7,23,24] and the exchange–correlation interactions are treated by the Perdew–Burke–Ernzerhof (PBE) functional.[25] Although the PBE functional is known to underestimate the band gap of semiconductors,[26] it can correctly predict the trends and physical mechanisms,[27] while the more accurate HSE functional[28] is not computationally affordable for large systems.[29] To consider the van der Waals forces, a DFT-D2 dispersion–correlation approach[30] is used, which is widely adopted in the graphdiyne related systems.[18,24,31,32] The rotationally invariant formulation of the on-site Hubbard-U model[33] is utilized at the Co sites with a U–J value of 3.3 eV.[34] The first Brillouin zone is sampled with the k-points using the Monkhorst–Pack scheme[35] with a grid density of $2\pi \times 0.02$ Å^{-1}, and the convergence criteria of 10^{-4} eV for total energy and 0.01 eV Å^{-1} for atomic forces are used. A large vacuum space of ~20 Å in the perpendicular direction is used to avoid the interactions between the periodic images. The Bader charge analysis[36] is carried out to quantitatively study the electron transfer. *Ab initio* molecular dynamics (AIMD) simulations are performed to study the passing-through events[37] of Li and the EC molecule through the pores in graphdiyne by using the NVT ensemble with the Nosé heat bath method[38] at 300 K.

Results and discussion

In Fig. 1, we show the geometrical structures of graphdiyne, a Li atom and an EC molecule to qualitatively analyze the permeability of the Li atom and the EC molecule through the pores of graphdiyne. Graphdiyne is composed of sp^2-hybridized carbon atoms (denoted as C_1 in Fig. 1(a)), and two types of sp-hybridized carbon atoms (denoted as C_2 and C_3), and the existence of sp-hybridized bonds between C_2 and C_3 carbon atoms makes the structure porous with ultralow areal density, as shown in Fig. 1(a). The optimized lattice constant is 9.45 Å, which is consistent with previous studies,[23,39] and the van der Waals pore size of graphdiyne is estimated to be 3.90 Å by considering the van der Waals radius of the acetylenic carbon (1.60 Å).[40] The van der Waals diameter of a freestanding Li atom is 3.64 Å,[40] which is smaller than 3.90 Å and favors the penetration.[14] The Bader charge analysis shows that a Li atom would transfer 0.90 e$^-$ to graphdiyne, further reducing the size of Li.[41] For EC, although it is the smallest molecule among common organic electrolytes ($EC(C_3H_4O_3)$, $PC(C_5H_7O_6)$, $DEC(C_5H_{10}O_3)$, $DMC(C_3H_6O_3)$, $EMC(C_4H_8O_3)$),[1] as indicated in Fig. 1(c), its size is too big to penetrate the pores in graphdiyne.

In order to quantitatively study the penetration behavior of Li and EC through the graphdiyne pores, the interaction energy profiles for Li and EC approaching the pores in graphdiyne are calculated. The results are presented in Fig. 2(a) and (b), which show a barrierless penetration of the Li atom through graphdiyne, and a high energy barrier of 2.18 eV for the EC molecule to overcome when approaching the graphdiyne plane. The easy penetration of Li should allow us to observe passing-through events[37] within the AIMD simulations. We introduce 16 Li atoms in a $4 \times 4 \times 1$ graphdiyne supercell ($Li_{16}C_{288}$) to perform the AIMD simulation at 300 K. As shown in Fig. 2(c), during the simulations of 10 picoseconds, the passing-through events for a Li atom are observed on average 64 times, which corresponds to a passage rate[42] of 6.4×10^{12} s^{-1}. The ultrahigh passage rate suggests ultrafast Li penetration through the graphdiyne plane as compared to that of the typical coating materials listed in Table 1, which results from the zero energy barrier and the ultrathin nature of graphdiyne. Similar AIMD simulations for EC molecules are also performed. However, as illustrated in Fig. 2(d), no passing-through event is observed during the same simulation time frame, which indicates that graphdiyne can effectively block the direct contact between EC and the electrodes. We also set a control group of Li passing-through the graphene plane with divacancies based on AIMD simulations. The results are plotted in Fig. S1 in the ESI.† Again no passing-through event is observed, implying that graphene cannot allow Li penetration, and is not suitable for electrode coating.

To understand the underlying mechanisms that govern the ultrahigh passage rate for Li and the no passing through effect for EC on graphdiyne, we plot the electron density distributions with $z = 0$ Å in Fig. 2(e) and (f). We note that there is little

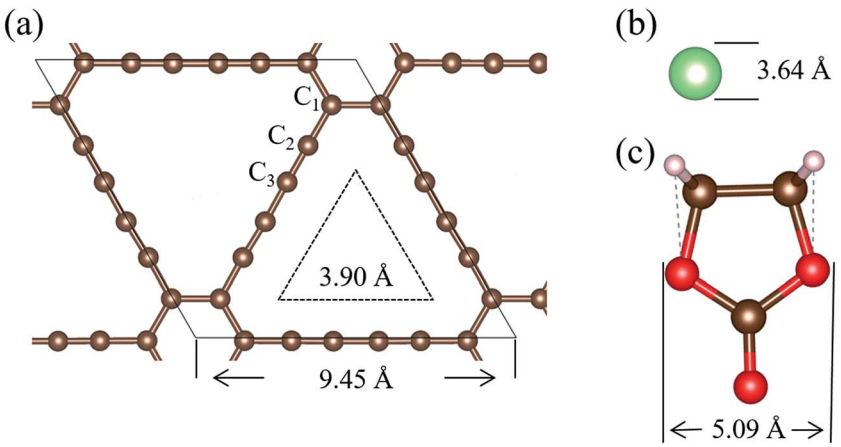

Fig. 1 (a–c) Structures of graphdiyne, a Li atom and an EC molecule, respectively. Color coding: C: brown; Li: green; O: red; H: pink.

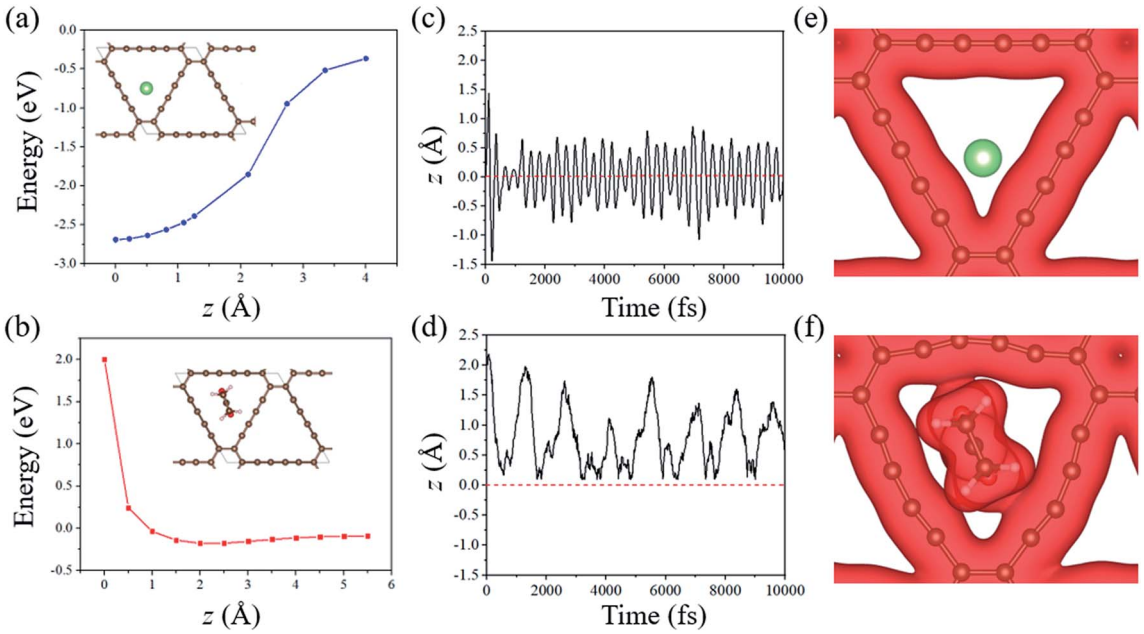

Fig. 2 (a) and (b) Potential energy profiles of a Li atom and an EC molecule approaching the pores in graphdiyne, respectively. z denotes the distance between the geometric center of Li/EC and the graphdiyne plane. The inset images show the configurations of Li/EC approaching graphdiyne. The orientation of EC shown here is the one with the lowest barrier among five trial configurations, and the other four orientations are provided in the ESI.† (c) and (d) Time-dependent distance between a Li atom/an EC molecule and the graphdiyne plane during the AIMD simulations, respectively. (e) and (f) electron density distributions with an iso value of 0.02 Bohr Å^{-3} for the states where $z = 0$ Å.

overlap between the electron densities of the Li atom and graphdiyne, and the geometry of graphdiyne remains almost intact, showing that Li can easily penetrate the graphdiyne layer. However a huge lattice distortion of graphdiyne and a large overlap between the electron densities of the EC molecule and the pore rim of graphdiyne occur when accommodating an EC molecule, hindering the penetration of the EC molecule through the graphdiyne plane. In previous studies, it has also been found that the molecules with higher penetration barriers exhibit more pronounced electron density overlap with the pores in nanosheets.[18,44]

In order to evaluate the electrochemical stability, the electrochemical window of graphdiyne is determined using the following scheme:[9]

$$C_{18} + \delta Li^+ + \delta e^- \rightarrow Li_\delta C_{18},\ eV_d = E(C_{18}) + E(\delta Li^+) + E(\delta e^-) - E(Li_\delta C_{18}) \quad (1)$$

$$C_{18} \rightarrow C_{18-\delta} + \delta C^+ + \delta e^-,\ eV_c = E(C_{18-\delta}) + E(\delta C^+) + E(\delta e^-) - E(C_{18}) \quad (2)$$

where reaction (1) is the possible Li adsorption reaction on graphdiyne (denoted as C_{18} in reactions (1) and (2) as one graphdiyne primitive cell consists of 18 carbon atoms) during the discharge process, reaction (2) is the first step of the possible decomposition reaction of graphdiyne during the charge process, δ denotes a dilute amount, E represents the total energy of each system, and V_d and V_c are the highest discharge potential and the lowest charge potential with regard to the Li^+/Li anode, respectively. A more detailed discussion about reaction (2) is provided in the ESI.† The operating voltages of coated electrodes should be larger than V_d and smaller than V_c for graphdiyne to remain electrochemically inactive. Here, we build a $2 \times 2 \times 1$ graphdiyne supercell as the initial state and estimate the reactions by adding one Li atom or removing one carbon atom (corresponding to $\delta = 0.25$ in reactions (1) and (2), and removing different types of carbon atoms does not change the value of V_c), and get $V_d = 1.02$ V and $V_c = 7.85$ V, which covers the operating voltages of some anodes[45,46] and most cathodes.[1] The width of the window (6.83 V) is also bigger than that of most organic electrolytes[1] and much larger than that of the narrowest acceptable window for cathode coatings (0.5 V),[9] showing the high electrochemical stability of graphdiyne.

$LiCoO_2$, as the cathode material for most commercial Li-ion batteries,[4] possesses the operating voltages (3.0 V to 4.4 V)[47]

Table 1 Diffusion barriers (in eV) and the estimated passage rate at 300 K (in s^{-1}) of Li in graphdiyne and some typical coating materials with assumed thicknesses of 1 nm

Material	Graphdiyne	Al_2O_3 (ref. 11)	AlF_3 (ref. 11)	MgO (ref. 11)	ZrO_2 (ref. 11)	TiO_2 (ref. 43)
Diffusion barrier	0	0.73	0.65	1.42	0.96	1.31
Passage rate	6.4×10^{12}	2.9	65	7.5×10^{-12}	4.0×10^{-4}	5.5×10^{-10}

Table 2 Structural details of the heterostructures composed of graphdiyne and the (101), (104) and (012) surfaces of $LiCoO_2$. *a*, *b* and θ represent the superlattice parameters, and *N* denotes the number of atoms in the supercells. The lattice mismatches between graphdiyne and the surfaces are given inside the parentheses

	Graphdiyne	$LiCoO_2$ (101)	$LiCoO_2$ (104)	$LiCoO_2$ (012)
a	9.45 Å	9.97 Å (5.2%)	11.8 Å (19.9%)	10.4 Å (9.1%)
b	16.37 Å	16.92 Å (3.3%)	16.92 Å (3.3%)	16.92 Å (3.3%)
θ	90°	90°	90°	90°
N	36	192	180	192

deep inside the electrochemical window of graphdiyne, and a band gap of 1.02 eV (ref. 4) at the PBE level. As an example, we choose $LiCoO_2$ as the electrode to study the bonding and electronic properties of graphdiyne-coated electrodes. Three nonpolar surfaces of $LiCoO_2$, namely the (101), (104) and (012) surfaces, are experimentally observed to be the preferential surfaces.[48–50] Based on Zur-McGill's scheme,[51] we build three heterostructures by stacking the graphdiyne monolayer and the three surfaces of $LiCoO_2$, respectively. The surfaces are modeled using the four-layer $LiCoO_2$ slab supercells with thicknesses of around 9 Å. The total number of atoms in the heterostructures is set to be less than 250 because DFT calculations are not tractable for large systems. The structural details of the heterostructures are listed in Table 2. It is obvious that the lattice mismatch between graphdiyne and the $LiCoO_2$ (101) surface is acceptable within the limited number of atoms, because it is less than the ultimate strain of graphdiyne (6.3%),[52] while in the other two cases, the large strains would cause structural failure of graphdiyne in the heterostructure models. Therefore, we further study the heterostructure composed of graphdiyne and the $LiCoO_2$ (101) surface.

In the heterostructure, we choose to stretch the graphdiyne supercell to match the $LiCoO_2$ surface supercell because of its high ductility and low atomic ratio in the model, and we keep the positions of the bottom two layers of $LiCoO_2$ fixed while relaxing that of all other atoms. The optimized structure is plotted in Fig. 3(a) and (b), which show no significant distortion in the geometry of graphdiyne after optimization, implying that the lattice strain is not destructive in this model. Then we study the bonding strength by calculating the binding energy, which is defined as:

$$E_b = (E_H - E_G - E_L)/n \quad (3)$$

where E_H is the total energy of the heterostructure, E_G and E_L are the total energies of the graphdiyne and the $LiCoO_2$ slab supercells, respectively, and *n* represents the number of carbon atoms in graphdiyne. Fig. 3(c) shows the binding energy as a function of the interlayer distance. The equilibrium interlayer distance is found to be 2.05 Å with a binding energy of 0.19 eV per atom. The bonding feature is similar to that of graphdiyne/Pt, Ni, Pd heterostructures,[53] and shows a stronger binding than some typical van der Waals crystals such as graphite (3.33 Å, 0.052 eV per atom) and h-BN (3.33 Å, 0.065 eV per atom). Moreover, the bonding is stronger than that of graphdiyne on the Cu (111) surface (3.21 Å, 0.11 eV per atom),[53] and is much stronger than that of bilayer graphdiyne (3.42 Å, 0.030 eV per atom),[39] suggesting that it is energetically favorable to transfer graphdiyne from Cu (111) to $LiCoO_2$ (101) or to directly synthesize the complex of graphdiyne on the $LiCoO_2$ (101) surface, and it is much more preferable for graphdiyne to cover the whole $LiCoO_2$ (101) surface than form the multilayer structure, which is beneficial to uniform coating.

In order to understand the bonding mechanism, we calculate the electrostatic potential and charge density difference of the heterostructure composed of graphdiyne and the $LiCoO_2$ surface. The results are presented in Fig. 4(a) and (b). Fig. 4(a) shows that graphdiyne has a much deeper electrostatic potential than the $LiCoO_2$ surface, implying that electrons tend to transfer from the $LiCoO_2$ surface to graphdiyne, and after contact electron leakage to the electrolytes becomes more difficult because electrons are trapped in a deeper potential well. The Bader charge analysis shows that after contact graphdiyne gains 0.05 e^- per atom on average; among them C_1 carbon atoms gain 0.02 e^- per atom, C_2 carbon atoms gain 0.20 e^- per atom while C_3 carbon atoms lose 0.06 e^- per atom with respect to the charges in free standing graphdiyne. The magnitude of electron transfer here is larger than that of typical

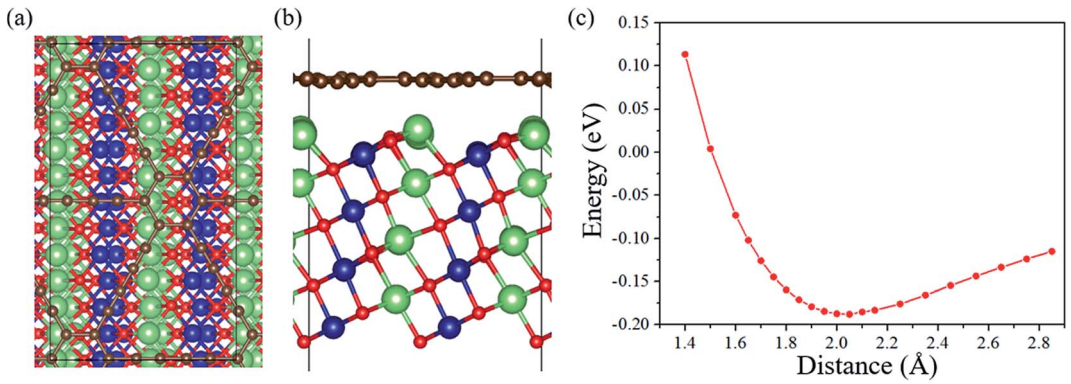

Fig. 3 (a) Top and (b) side views of the optimized heterostructure composed of graphdiyne and the $LiCoO_2$ (101) surface. (c) Binding energy as a function of the interlayer distance between the graphdiyne monolayer and the $LiCoO_2$ surface. Color coding: C: brown; Li: green; Co: dark blue; O: red.

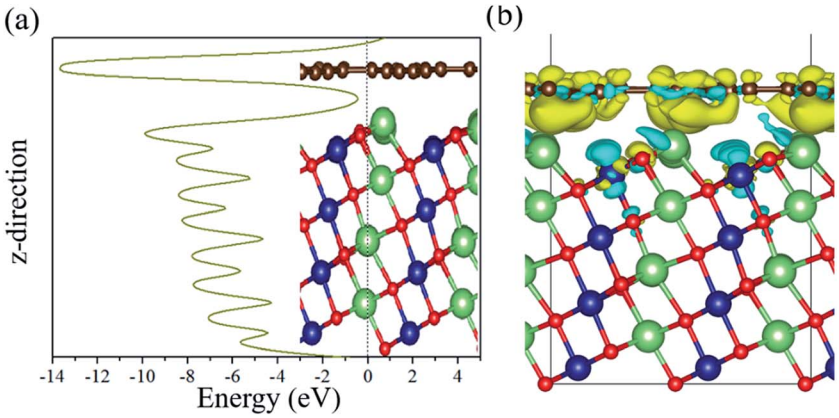

Fig. 4 (a). Electrostatic potential of the graphdiyne/$LiCoO_2$ (101) surface heterostructure. (b) Charge density difference with an iso value of 0.002 Bohr $Å^{-3}$ by subtracting the electronic charge of the heterostructure from those of the graphdiyne and $LiCoO_2$ (101) surface. Yellow: electron accumulation; blue: electron depletion.

van der Waals heterostructures like graphene/black phosphorene (0.003 e^- per atom)[54] and graphene/MoS_2 (0.02 e^- per atom),[55] again suggesting a strong interaction between graphdiyne and the $LiCoO_2$ (101) surface. Fig. 4(b) shows that in the surface layer of $LiCoO_2$, Co atoms and Li atoms lose electrons and O atoms acquire electrons, implying the redistribution of surface dangling bonds. Here two kinds of atoms with small electronegativities lose electrons (Li: 0.98; Co: 1.88), while the others with large electronegativities gain electrons (C: 2.55; O: 3.44).[27] This trend raises the expectation that other $LiCoO_2$-like electrodes, such as $LiMnO_2$ (Mn: 1.55) and $LiNiO_2$ (Ni: 1.91),[56] might share similar interfacial bonding characters with $LiCoO_2$ when coated with graphdiyne. Moreover, as a result of large electron transfer and strong interaction[54] between graphdiyne and $LiCoO_2$, as shown in Fig. 4(a) there is no tunneling barrier appearing at the graphdiyne/$LiCoO_2$ interface, which is similar to the case in graphdiyne/Pd contact[53] and would result in a low interfacial electron resistance with a 100% electron tunneling possibility.[53,57]

Finally, the density of states (DOS) of the freestanding graphdiyne and the $LiCoO_2$ (101) slab, and the DOS of the graphdiyne and the $LiCoO_2$ slab supercells in the heterostructure model are calculated and plotted in Fig. 5. The band gap of 0.48 eV of freestanding graphdiyne is close to that of a previous study (0.46 eV),[23] while the band gap of the freestanding $LiCoO_2$ slab (0.73 eV) is smaller than that of the bulk material (1.02 eV),[4] which is common in slab model calculations.[58] However, after contact both of the two components in the heterostructure transform from semiconductors into metals: as mentioned above, the $LiCoO_2$ slab loses electrons to graphdiyne, and as a result the Fermi level moves downward into the valence band, which is equivalent to a p-type doping and known to notably improve the electronic conductivity of $LiCoO_2$;[59] as for graphdiyne, in the heterostructure model it gains electrons from $LiCoO_2$, leading to the metallization[57] of graphdiyne and with more electronic states near the Fermi level, the electronic conductivity of graphdiyne is also improved. Together with the aforementioned low interfacial resistance between graphdiyne and the $LiCoO_2$ slab, we believe that the graphdiyne coating would improve the electronic conductivity of $LiCoO_2$.

Based on the above discussions, it is clear that graphdiyne can bond tightly with the $LiCoO_2$ surface and improve the electronic conductivity of $LiCoO_2$. To demonstrate the general suitability of graphdiyne coating, we need to prove that during the charging/discharging process, the binding between graphdiyne and Li_xCoO_2 ($0 < x < 1$) remains strong. To this end, we choose $Li_{0.5}CoO_2$ as an example of the intermediate states, because lithium intercalation/deintercalation is reversible only in the compositional range of $LiCoO_2$–$Li_{0.5}CoO_2$.[60] However for other widely used cathode materials, we choose $LiMn_{0.5}Ni_{0.5}O_2$ (ref. 61) and $LiFePO_4$ (ref. 6) as other two examples. The electron work functions of graphdiyne, $LiCoO_2$ (101), $Li_{0.5}CoO_2$ (101), $LiMn_{0.5}Ni_{0.5}O_2$ (101), and $LiFePO_4$ (010) (preferable surface[62]) surfaces are calculated, and the results are given in Fig. S3 in the ESI.† The larger the difference of electron work functions, the more the charge transfer, and the stronger the binding between the coating layer and the cathode. The electron work function of the $Li_{0.5}CoO_2$ (101) surface is found to be slightly larger than that of the $LiCoO_2$ (101) surface, but much smaller than that of graphdiyne, which indicates that when coated with graphdiyne, the $Li_{0.5}CoO_2$ (101) surface would share similar interaction behaviors with the fully Li-intercalated state. For the $LiMn_{0.5}Ni_{0.5}O_2$ (101) surface, its electron work function is also slightly larger than that of the $LiCoO_2$ (101) surface and much smaller than that of graphdiyne. However the electron work function of the $LiFePO_4$ (010) surface is even smaller than that of the $LiCoO_2$ (101) surface. This suggests that besides $LiCoO_2$ (101), graphdiyne can also be used as a coating material for $LiMn_{0.5}Ni_{0.5}O_2$ and $LiFePO_4$.

In addition to considering the interaction, we study the volumetric change of $LiCoO_2$. We find that, as compared to $LiCoO_2$, the volume of $Li_{0.5}CoO_2$ expands only 1.34%, which is consistent with the previous work,[63] and the lattice mismatch between graphdiyne and the $Li_{0.5}CoO_2$ (101) surface is 5.3% and 3.4% in the *a* and *b* directions, respectively, as shown in Table 2, which are very close to the values of the $LiCoO_2$ (101) surface, and smaller than the ultimate strain of graphdiyne (6.3%),

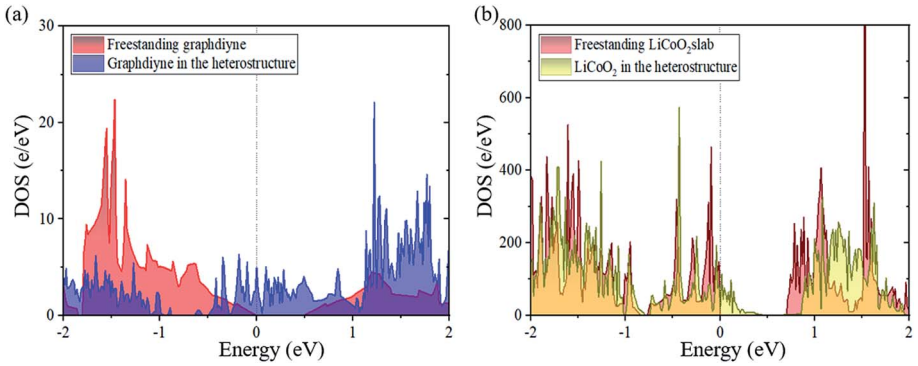

Fig. 5 (a) DOS of freestanding graphdiyne and that of graphdiyne in the heterostructure model. (b) DOS of freestanding $LiCoO_2$ (101) surface and that of the $LiCoO_2$ slab supercell in the heterostructure model. The Fermi levels are set to be 0 eV.

indicating that graphdiyne coating could bear the volumetric change during the charge/discharge process of $LiCoO_2$. Therefore, we demonstrate that as a coating material, graphdiyne remains tightly bound with the cathode $LiCoO_2$ surface during charging and discharging processes, and it can also be coated on $Li_{0.5}CoO_2$, $LiMn_{0.5}Ni_{0.5}O_2$ and $LiFePO_4$ surfaces.

Conclusions

In summary, we show that graphdiyne can be considered as an ideal monolayer coating material for LIB cathodes because it meets all the basic requirements and exhibits ultrafast Li diffusion and ultralow areal density. Based on extensive DFT calculations, we find that graphdiyne can bind the $LiCoO_2$ surface with a large binding energy of 0.19 eV per C atom, which is beneficial to uniform coating and close attachment. Graphdiyne can allow Li penetration without energy barrier, while it blocks the direct contact between electrodes and the EC molecule. Moreover, graphdiyne shows a high electrochemical stability with a wide electrochemical window of 6.83 V, and the graphdiyne coating enhances the electronic conductivity of semiconducting electrodes. We further demonstrate that our findings based on $LiCoO_2$ are also suitable for $Li_{0.5}CoO_2$, $LiMn_{0.5}Ni_{0.5}O_2$ and $LiFePO_4$. These features are favorable for large specific capacity, high rate performance and long cycling life for LIBs.

Conflicts of interest

The authors declare no competing financial interests.

Acknowledgements

This work is supported by grants from the National Key Research and Development Program of China (2016YFE0127300, and 2017YFA0205003), the National Natural Science Foundation of China (NSFC-51471004, and NSFC-21773004), the National Training Program of Innovation for Undergraduates of China (201611001008), and supported by the High Performance Computing Platform of Peking University, China.

References

1 J. B. Goodenough and Y. Kim, *Chem. Mater.*, 2010, **22**, 587–603.
2 X. Meng, X. Q. Yang and X. Sun, *Adv. Mater.*, 2012, **24**, 3589–3615.
3 W.-M. Zhang, J.-S. Hu, Y.-G. Guo, S.-F. Zheng, L.-S. Zhong, W.-G. Song and L.-J. Wan, *Adv. Mater.*, 2008, **20**, 1160–1165.
4 B. Andriyevsky, K. Doll and T. Jacob, *Phys. Chem. Chem. Phys.*, 2014, **16**, 23412–23420.
5 H. Li and H. Zhou, *Chem. Commun.*, 2012, **48**, 1201–1217.
6 J. Wang and X. Sun, *Energy Environ. Sci.*, 2012, **5**, 5163–5185.
7 B. Zhang, Y. Yu, Y. Liu, Z. D. Huang, Y. B. He and J. K. Kim, *Nanoscale*, 2013, **5**, 2100–2106.
8 K. Min, S. W. Seo, B. Choi, K. Park and E. Cho, *ACS Appl. Mater. Interfaces*, 2017, **9**, 17822–17834.
9 M. Aykol, S. Kim, V. I. Hegde, D. Snydacker, Z. Lu, S. Hao, S. Kirklin, D. Morgan and C. Wolverton, *Nat. Commun.*, 2016, **7**, 13779.
10 X. Xiao, P. Lu and D. Ahn, *Adv. Mater.*, 2011, **23**, 3911–3915.
11 S. Xu, R. M. Jacobs, H. M. Nguyen, S. Hao, M. Mahanthappa, C. Wolverton and D. Morgan, *J. Mater. Chem. A*, 2015, **3**, 17248–17272.
12 G. Li, Y. Li, H. Liu, Y. Guo, Y. Li and D. Zhu, *Chem. Commun.*, 2010, **46**, 3256–3258.
13 W. Wan and H. D. Wang, *Materials*, 2015, **8**, 6163–6178.
14 H. Zhang, Y. Xia, H. Bu, X. Wang, M. Zhang, Y. Luo and M. Zhao, *J. Appl. Phys.*, 2013, **113**, 044309.
15 R. E. Roman and S. W. Cranford, *Adv. Eng. Mater.*, 2014, **16**, 862–871.
16 Y. Pei, *Phys. B*, 2012, **407**, 4436–4439.
17 F. Diederich and Y. Rubin, *Angew. Chem., Int. Ed.*, 1992, **31**, 1101–1123.
18 Z. Meng, X. Zhang, Y. Zhang, H. Gao, Y. Wang, Q. Shi, D. Rao, Y. Liu, K. Deng and R. Lu, *ACS Appl. Mater. Interfaces*, 2016, **8**, 28166–28170.
19 X. Cui, P. Ren, D. Deng, J. Deng and X. Bao, *Energy Environ. Sci.*, 2016, **9**, 123–129.
20 J. Mahmood, S.-M. Jung, S.-J. Kim, J. Park, J.-W. Yoo and J.-B. Baek, *Chem. Mater.*, 2015, **27**, 4860–4864.

21 G. Kresse and J. Furthmuller, *Phys. Rev. B*, 1996, **54**, 11169–11186.
22 P. E. Blochl, *Phys. Rev. B*, 1994, **50**, 17953–17979.
23 M. Q. Long, L. Tang, D. Wang, Y. L. Li and Z. G. Shuai, *ACS Nano*, 2011, **5**, 2593–2600.
24 Z. Xu, X. Lv, J. Li, J. Chen and Q. Liu, *RSC Adv.*, 2016, **6**, 25594–25600.
25 J. P. Perdew, K. Burke and M. Ernzerhof, *Phys. Rev. Lett.*, 1996, **77**, 3865–3868.
26 Z. L. Guo, N. H. Miao, J. Zhou, B. S. Sa and Z. Sun, *J. Mater. Chem. C*, 2017, **5**, 978–984.
27 C. X. Xia, B. Xue, T. X. Wang, Y. T. Peng and Y. Jia, *Appl. Phys. Lett.*, 2015, **107**, 193107.
28 J. E. Moussa, P. A. Schultz and J. R. Chelikowsky, *J. Chem. Phys.*, 2012, **136**, 204117.
29 P. Ganesh, P. R. C. Kent and D.-e. Jiang, *J. Phys. Chem. C*, 2012, **116**, 24476–24481.
30 S. Grimme, *J. Comput. Chem.*, 2006, **27**, 1787–1799.
31 Y. Jiao, A. Du, S. C. Smith, Z. Zhu and S. Z. Qiao, *J. Mater. Chem. A*, 2015, **3**, 6767–6771.
32 B. K. Das, D. Sen and K. K. Chattopadhyay, *Phys. Chem. Chem. Phys.*, 2016, **18**, 2949–2958.
33 S. L. Dudarev, G. A. Botton, S. Y. Savrasov, C. J. Humphreys and A. P. Sutton, *Phys. Rev. B*, 1998, **57**, 1505–1509.
34 L. Wang, T. Maxisch and G. Ceder, *Phys. Rev. B*, 2006, **73**, 195107.
35 H. J. Monkhorst and J. D. Pack, *Phys. Rev. B*, 1976, **13**, 5188–5192.
36 W. Tang, E. Sanville and G. Henkelman, *J. Phys.: Condens. Matter*, 2009, **21**, 084204.
37 D. E. Jiang, V. R. Cooper and S. Dai, *Nano Lett.*, 2009, **9**, 4019–4024.
38 W. Chung Lo and B. Li, *J. Phys. Soc. Jpn.*, 2010, **79**, 074402.
39 Q. Zheng, G. Luo, Q. Liu, R. Quhe, J. Zheng, K. Tang, Z. Gao, S. Nagase and J. Lu, *Nanoscale*, 2012, **4**, 3990–3996.
40 A. Bondi, *J. Phys. Chem.*, 1964, **68**, 441–451.
41 D. Q. Er, J. W. Li, M. Naguib, Y. Gogotsi and V. B. Shenoy, *ACS Appl. Mater. Interfaces*, 2014, **6**, 11173–11179.
42 K. Sint, B. Wang and P. Kral, *J. Am. Chem. Soc.*, 2008, **130**, 16448–16449.
43 F. Tielens, M. Calatayud, A. Beltrán, C. Minot and J. Andrés, *J. Electroanal. Chem.*, 2005, **581**, 216–223.
44 Y. Li, Z. Zhou, P. Shen and Z. Chen, *Chem. Commun.*, 2010, **46**, 3672–3674.
45 S. Gong and Q. Wang, *J. Phys. Chem. C*, 2017, **121**, 24418–24424.
46 S. Gong, C. Zhang, S. Wang and Q. Wang, *J. Phys. Chem. C*, 2017, **121**, 10258–10264.
47 Y. Sun, J. Han, S. Myung, S. Lee and K. Amine, *Electrochem. Commun.*, 2006, **8**, 821–826.
48 L. Bohne, T. Pirk and W. Jaegermann, *J. Solid State Electrochem.*, 2011, **17**, 2095–2099.
49 M. Yoshio, H. Tanaka, K. Tominaga and H. Noguchi, *J. Power Sources*, 1992, **40**, 347–353.
50 R. Kohler, J. Proell, S. Ulrich, V. Trouillet, S. Indris, M. Przybylski and W. Pfleging, *Proc. SPIE*, 2009, **7202**, 720207.
51 A. Zur and T. C. McGill, *J. Appl. Phys.*, 1984, **55**, 378–386.
52 S. W. Cranford, D. B. Brommer and M. J. Buehler, *Nanoscale*, 2012, **4**, 7797–7809.
53 Y. Pan, Y. Wang, L. Wang, H. Zhong, R. Quhe, Z. Ni, M. Ye, W. N. Mei, J. Shi, W. Guo, J. Yang and J. Lu, *Nanoscale*, 2015, **7**, 2116–2127.
54 Y. Cai, G. Zhang and Y.-W. Zhang, *J. Phys. Chem. C*, 2015, **119**, 13929–13936.
55 W. Hu, T. Wang, R. Q. Zhang and J. L. Yang, *J. Mater. Chem. C*, 2016, **4**, 1776–1781.
56 L. M. Yan, J. M. Su, C. Sun and B. H. Yue, *Adv. Manuf.*, 2014, **2**, 358–368.
57 Y. Pan, Y. Wang, M. Ye, R. Quhe, H. Zhong, Z. Song, X. Peng, D. Yu, J. Yang, J. Shi and J. Lu, *Chem. Mater.*, 2016, **28**, 2100–2109.
58 F. Wang, C. Di Valentin and G. Pacchioni, *J. Phys. Chem. C*, 2012, **116**, 10672–10679.
59 S. Shi, C. Ouyang, M. Lei and W. Tang, *J. Power Sources*, 2007, **171**, 908–912.
60 J. Molenda, *Funct. Mater. Lett.*, 2011, **04**, 107–112.
61 B.-J. Hwang, S.-K. Hu, C.-H. Chen, C.-Y. Chen and H.-S. Sheu, *J. Power Sources*, 2007, **174**, 761–765.
62 P. Zhang, D. Zhang, L. Huang, Q. Wei, M. Lin and X. Ren, *J. Alloys Compd.*, 2012, **540**, 121–126.
63 F. Xiong, H. J. Yan, Y. Chen, B. Xu, J. X. Le and C. Y. Ouyang, *Int. J. Electrochem. Sci.*, 2012, **7**, 9390–9400.

